Bulletin of the Seismological Society of America, Vol. 77, No. 2, pp. 631–662, April 1987

CRUSTAL STRUCTURE AT REGIONAL SEISMIC TEST NETWORK STATIONS DETERMINED FROM INVERSION OF BROADBAND TELESEISMIC *P* WAVEFORMS

BY THOMAS J. OWENS,* STEVEN R. TAYLOR, AND GEORGE ZANDT

ABSTRACT

The site structure beneath the five broadband stations of the Regional Seismic Test Network (RSTN) has been determined utilizing teleseismic *P* waveforms. Our teleseismic waveform modeling technique involves inverting the radial component of stacked source-equalized receiver functions in the time domain to estimate the vertical shear velocity structure at the site. The receiver functions at RSNY (Adirondacks, New York), RSON (Red Lake, Ontario), and RSNT (Yellowknife, Northwest Territory) are quite simple compared to previously published RSCP (Cumberland Plateau, Tennessee) data, largely due to the absence of sedimentary surface rocks at these sites. At RSNY, a high-velocity layer at mid-crustal depths (18 to 26 km) in our southeast backazimuth results correlates in depth with a zone of high-amplitude reflections found on COCORP profiles 60 km south of RSNY. A gradational crust-mantle boundary is observed at RSCP and RSNY. The RSON and RSNT sites are characterized by simple crusts with fairly abrupt crust-mantle boundaries. The crust beneath RSON appears to have a clear division between the upper and lower crust at about 18 km depth while this boundary is not well-developed at RSNT. Pronounced azimuthal variations in crustal structure at RSSD (Black Hills, South Dakota) prohibit the determination of velocity using a layered earth model. The crustal thicknesses at each of these sites are: RSCP, 40 to 50 km; RSSD, 47 to 50 km; RSNY, 45 to 50 km; RSNT, 38 km; and RSON, 42 km.

INTRODUCTION

The purpose of this paper is to summarize the final results of our study of the local crustal structure beneath the stations of the Regional Seismic Test Network (RSTN). The RSTN was established as part of the Department of Energy's Test Ban Treaty Verification Program as a prototype of a network which could be installed in the Soviet Union to monitor a Comprehensive Test Ban Treaty. Thus, the locations and separations of RSTN stations (Figure 1, Table 1) were chosen to simulate geological conditions that could be encountered in the Soviet Union. As part of the Lawrence Livermore National Laboratory's research program to evaluate the characteristics and performance of the RSTN, this study was undertaken to determine the site structure beneath all five stations of the network.

This paper summarizes the geologic and geophysical setting of each of the five borehole seismometer systems that comprise the RSTN. The teleseismic waveform modeling technique we have used has resulted in detailed velocity-depth profiles at each of the RSTN sites. Complete interpretations of these profiles are the subject of several other papers (Owens *et al.*, 1984; Owens and Zandt, 1985; Zandt and Owens, 1986; Owens, 1986). However, increased usage of RSTN data necessitates a complete summary of available information on the RSTN sites and this report is intended to provide this information. Following a brief description of our analysis techniques, we will discuss the site structures beneath RSTN stations. In addition, we provide in the Appendix a complete listing of our velocity-depth profiles for each site so that other RSTN data users may utilize them as needed.

* Present address: Department of Geology, University of Missouri, Columbia, Missouri 65211.

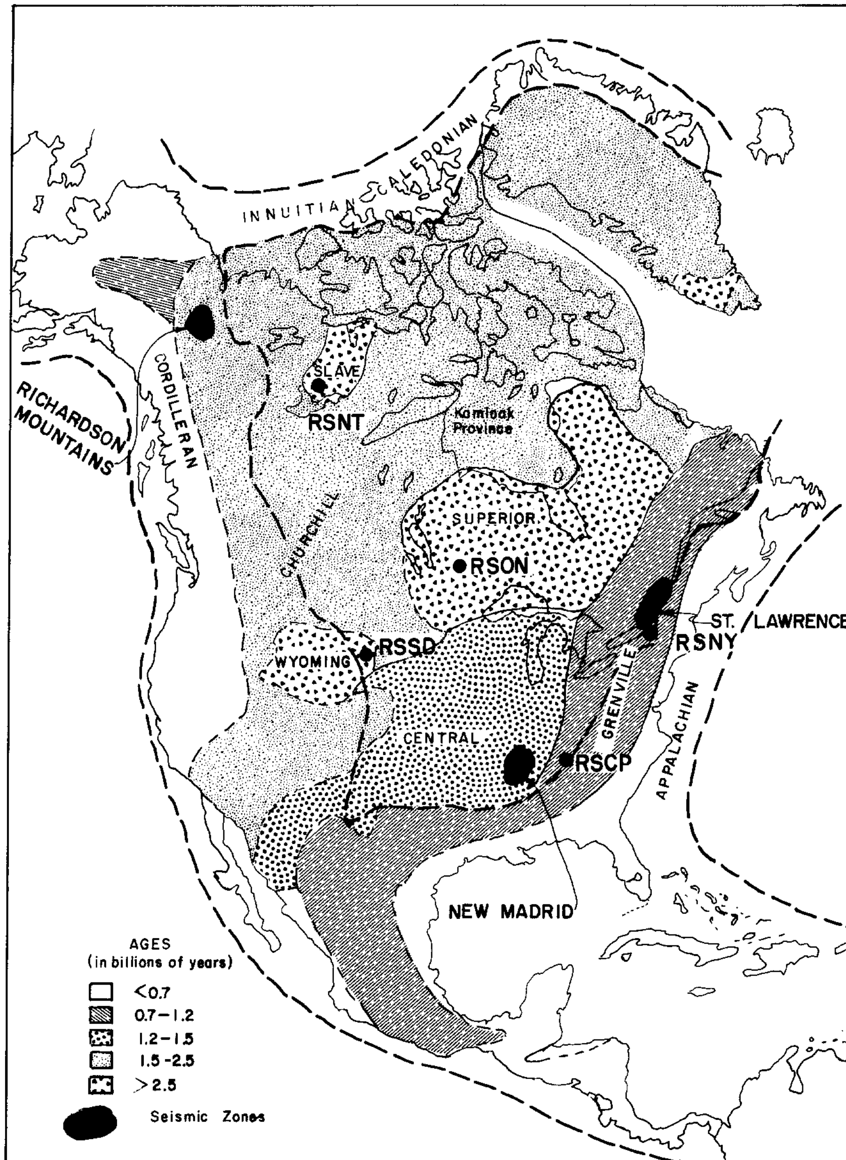

FIG. 1. Major crustal provinces in North America showing major Precambrian regions and RSTN stations but excluding anorogenic provinces. Inner and outer boundaries of Phanerozoic belts are shown with the heavy dashed lines.

TABLE 1
RSTN STATION LOCATIONS

Station	Latitude (°N)	Longitude (°W)
RSON	50.859	93.702
RSNT	62.480	114.592
RSCP	35.600	85.569
RSSD	44.120	104.036
RSNY	44.548	74.530

Broadband Teleseismic Waveform Analysis

Teleseismic body waveforms have often been used to infer crustal structure beneath isolated seismic stations (see for a review, Owens, 1984, or Owens *et al.*, 1984). Recently, we have refined and extended these techniques to take advantage of the new digital broadband seismograph stations in order to examine the detailed crustal and upper mantle structure beneath these stations (Owens, 1984; Owens *et al.*, 1984). We analyze teleseismic events recorded on the broad mid-period passband of the RSTN. This passband has a flat velocity response between 0.018 and 1.2 Hz. This broad bandwidth is an important aid to the resolution of our techniques (Owens *et al.*, 1984; Owens and Zandt, 1985).

To utilize teleseismic P waveforms, we must isolate the response of the crust and upper mantle velocity structure, the receiver function, from the source and path effects which also influence the recorded seismogram. Because we are primarily interested in converted waves of the P-to-S type (Figure 2), the horizontal components of the receiver function are isolated using a deconvolution procedure suggested by Langston (1979) and examined in detail by Owens *et al.* (1983a). In this process, original horizontal seismograms are rotated into radial and tangential components, and source effects are removed by deconvolving the vertical component from them. This approach assumes that the vertical component contains primarily the unwanted source and path effects, an assumption that can be justified (Owens *et al.*, 1983a). The deconvolved seismograms are then convolved with a simple Gaussian time function to produce smooth estimates of the horizontal receiver functions. We then gather many receiver function estimates from events clustered in both distance and backazimuth from a station and stack them to provide a single good quality estimate for each of the horizontal components.

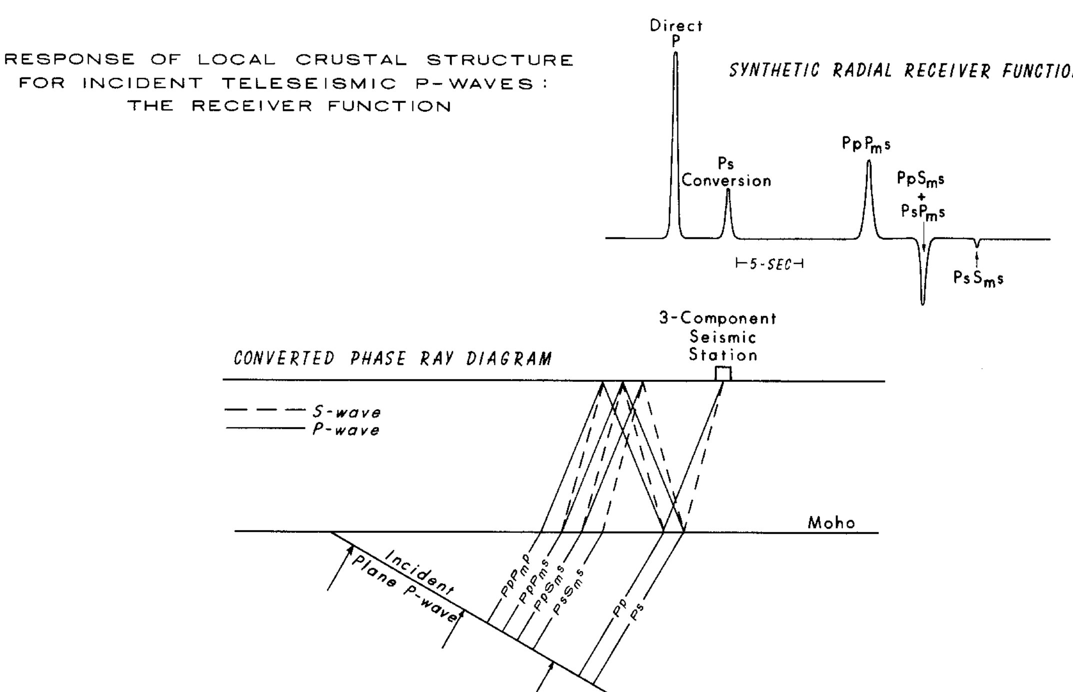

FIG. 2. Schematic of the effects of local structure on teleseismic P waves.

Modeling the detailed receiver functions obtained from broadband data required the development of a time-domain inversion routine. Initially, a frequency-domain approach using Thomson-Haskell propagator matrices was used, but proved to be too time-consuming for detailed calculations (Taylor and Owens, 1984). We assume a horizontally layered model and invert the radial receiver function for the vertical shear velocity structure at each backazimuth. The compressional velocities are obtained by assuming a Poisson's ratio of 0.25, and densities are adjusted using the equation $\rho = 0.32Vp + 0.77$ for layers below shallow sedimentary layers. The variation in these structures with azimuth allows us to examine gross lateral variations in structure around the station. This technique has provided strong evidence for tectonically significant velocities variations beneath two RSTN stations (Owens *et al.*, 1984; Owens, 1986). Details of the inversion process will not be discussed here and interested readers are referred to Owens (1984), Owens *et al.* (1984), and Taylor and Owens (1984).

RSTN Receiver Structures

In this section, we will discuss the crustal structures derived using our technique at the five RSTN stations. Because of strong lateral variations in structure in the Black Hills, detailed crustal models were not obtained for RSSD. Compared to RSCP, the three stations at RSNY, RSNT, and RSON have much simpler responses (Figure 3), largely due to their locations on the crystalline rock of the Canadian Shield and Adirondack Mountains (Figure 1), whereas RSCP is located in Paleozoic sedimentary rocks of the Cumberland Plateau. At RSNT, the lack of a sedimentary cover is combined with a remarkably simple crust to produce especially simple receiver functions. The high-velocity contrast commonly present at the contact between sedimentary and crystalline rocks can cause large amplitude phase conversions that arrive wihtin 2 to 3 sec of the direct P waves. These phases are clearly visible in the RSCP receiver functions (Figure 3) but since the sedimentary layers are relatively flat-lying, their existence beneath RSCP did not hinder our ability to resolve deeper structure. However, receiver functions at RSSD indicate that severe complications can arise at stations where the sedimentary layering is not horizontal. In the following, we review the results for each of the five RSTN stations. The Appendix contains tables of the velocity models of all results discussed in this report.

RSCP

The station RSCP is located on the Cumberland Plateau near McMinnville in central Tennessee. The Cumberland Plateau is characterized by relatively undeformed, nearly horizontal sedimentary rocks of Carboniferous age (Figure 4). The sedimentary sequences form part of the Pennsylvanian cyclothem and are composed of relatively thin-bedded limestones, sandstones, shales, and coal seams that dip gently to the east away from the westward-lying Nashville Dome. The Paleozoic sequence in the vicinity of RSCP is thought to be approximately 3 km thick and rests upon Precambrian Grenville rocks.

Major structures in the vicinity of the Cumberland Plateau include the Mississippi Embayment and Nashville Dome to the west, the Valley and Ridge marginal fold-and-thrust belt located about 70 km to the east, and the East-Continent Gravity High just to the north. The Valley and Ridge province forms the western limit of the southern Appalachian orogenic belt and is characterized by flexure folding and west-directed, thin-skinned thrusting involving early and mid-Paleozoic sediments

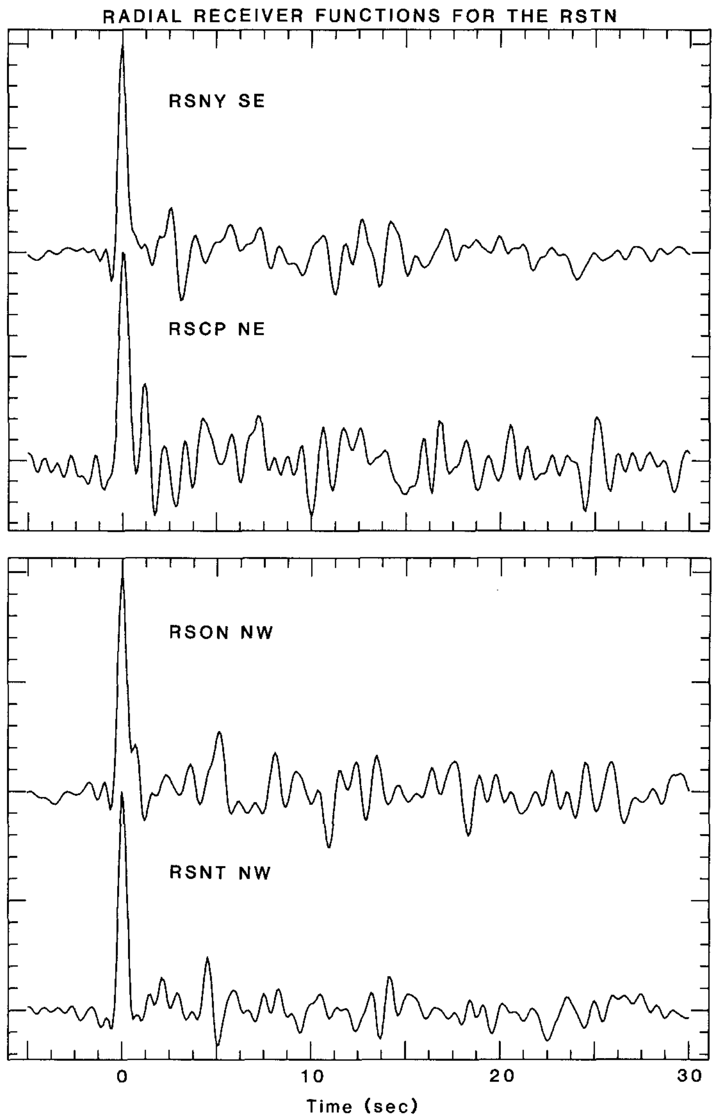

FIG. 3. Mean radial receiver functions at four RSTN sites. Zero time in this and all subsequent figures corresponds to the direct P-wave arrival.

(cf. Hatcher, 1978). Recent COCORP results indicate that much of the southern Appalachian orogenic belt is allochthonous and underlain by a basal decollement that extends from the Valley and Ridge as far east as the eastern Piedmont (Cook *et al.*, 1979). The East-Continent Gravity High extends to the northeast from the RSCP station vicinity and coincides with a zone of high-amplitude magnetic anomalies. Keller *et al.* (1982) suggest that the geophysical anomaly represents a Precambrian (Keweenawan) rift zone.

Prodehl *et al.* (1984) reinterpreted refraction lines of Borcherdt and Roller (1966) which cross at RSCP using stacking techniques to enhance the record stations and ray-tracing to match both primary and secondary arrivals. Upper crustal velocities of 6.1 to 6.2 km/sec were found overlying a 6.7 to 6.8 km/sec lower crust. A gradational boundary was postulated to separate the two layers between 7 to 10 km

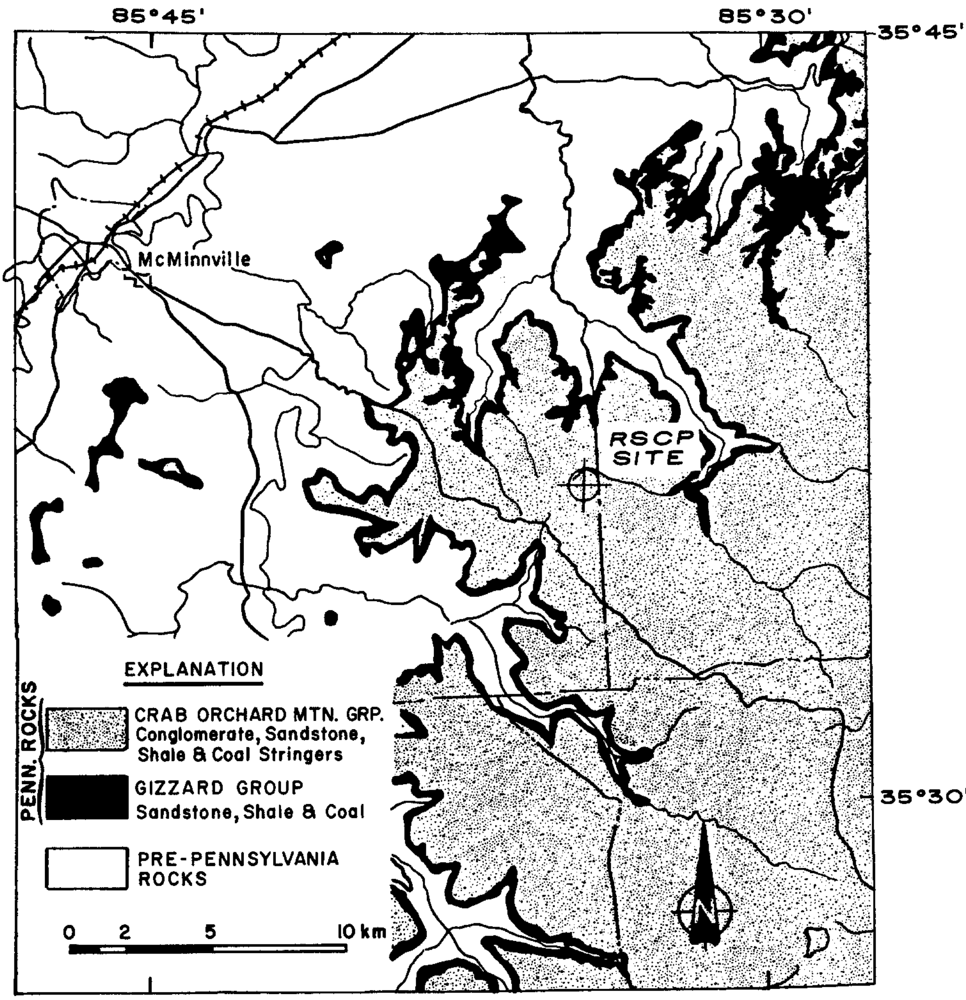

FIG. 4. Generalized geologic map of the RSCP site.

depth. From the lack of a clear *PmP* phase, a thick, gradational Moho was inferred to exist between 34 to 47 km depth, where velocities increased from 6.7 to 8.0 km/sec. To the northeast of RSCP, velocities in the upper 20 km were slightly greater than those beneath RSCP, but a high-velocity anomaly of the sort observed by our studies described below was not observed.

RSCP was the first RSTN station analyzed in this study. Because the results were published in Owens *et al.* (1984), we will only briefly review them here. Analysis of receiver functions at RSCP revealed significant rapid lateral variations in mid-crustal structure that have important tectonic implications (Owens *et al.*, 1984). In addition, the results showed variations in crustal and crust-mantle boundary structure quite consistent with results from seismic refraction data in the area (Prodehl *et al.*, 1984; Zandt and Owens, 1986). Radial receiver function inversions for the southeast and northeast backazimuths were of excellent quality (Figure 5). In this figure, and all other receiver function plots in this paper, the upper trace in each frame compares the derived synthetic response with the observed stacked mean radial receiver function while the lower frame plots the same synthetic along with two bounding receiver functions calculated by adding and subtracting one standard deviation from the mean at each time point. These bounds are quite useful indicators

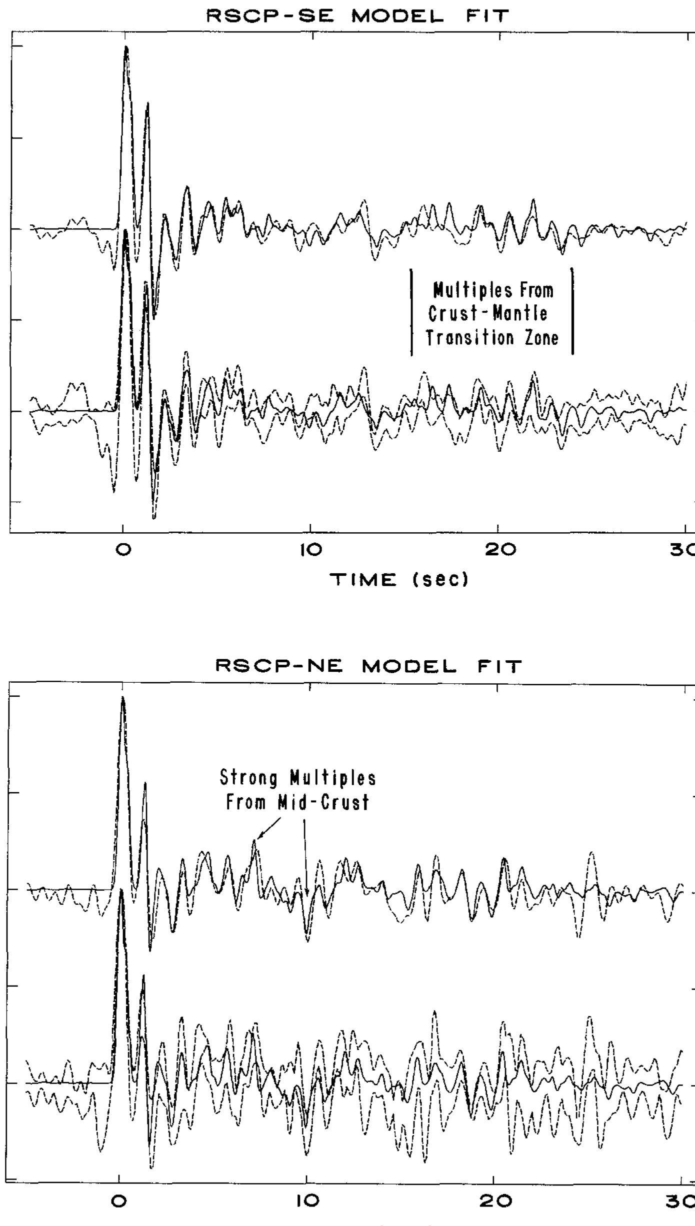

FIG. 5. Radial receiver function comparison of RSCP south-southeast (*top*) and northeast (*bottom*) backazimuths. Solid curves are derived synthetic; dashed curves are the data mean and bounds.

of the quality of the arrivals in the receiver function. At RSCP, the inversions at different backazimuths produced very different velocity-depth curves in the mid-crustal region (Figure 6). Owens *et al.* (1984) concluded that these variations were the result of RSCP's location near the southern terminus of the East Continent Gravity High (Keller *et al.*, 1982). Other interesting aspects of the RSCP results include the significant effects shallow structure has on mid-period data, as mentioned above, and the detailed structure of the crust-mantle boundary suggested by the receiver function inversions. This structure has been compared to other RSTN sites by Owens and Zandt (1985) and will be further discussed below.

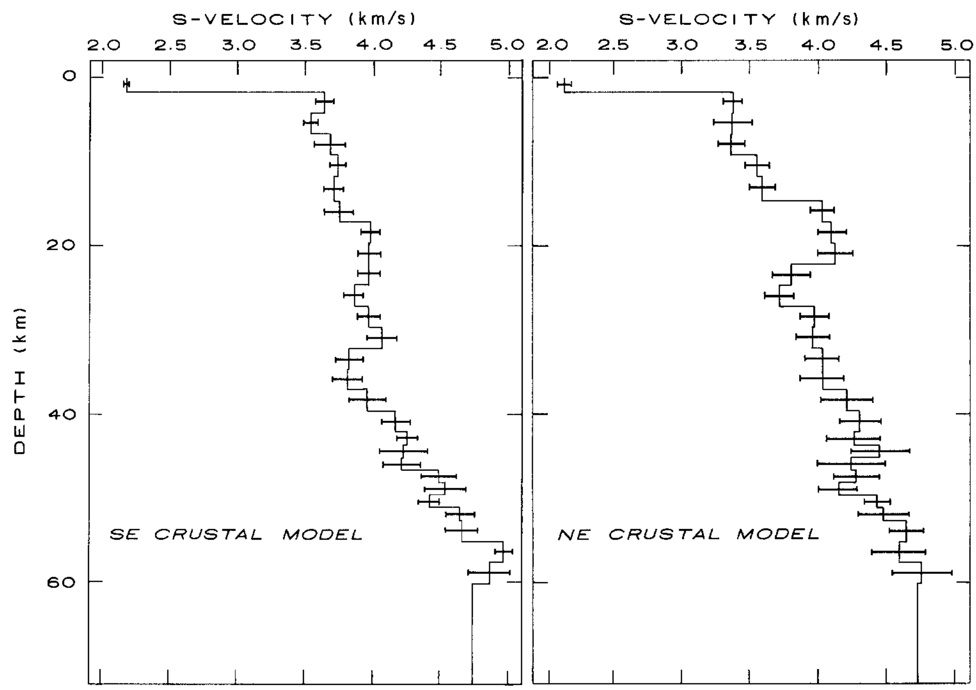

FIG. 6. Crustal models derived from waveform inversion of RSCP south-southeast (*left*) and northeast (*right*). Error bars represent ±2 S.E.

RSSD

The Black Hills form an elongate domal uplift exposing a core of Precambrian metamorphic and igneous rocks (Figure 7). The Precambrian rocks in the Black Hills give age dates of about 1.7 b.y. and are thought to correlate with those of the Churchill province. Some exposures of Archean granite on the northeastern edge of the range (Little Elk Granite, 2.5 b.y.) are thought to represent part of the basement upon which early Proterozoic sediments were deposited. The range is flanked by Paleozoic to Cretaceous sedimentary rocks ranging in composition from carbonates in the Paleozoic section to shales and sandstones in the uppermost Paleozoic to Cretaceous section. Tertiary igneous rocks (39 to 59 m.y.) and laccoliths are found in the northern portions of the Black Hills.

In cross-section, the Black Hills are asymmetrical and sedimentary units on the east flank generally dip off more steeply than those on the west flank. Because of this shallow dip on the west, the Limestone plateau is extensive to the west of the Precambrian core. In the vicnity of the RSSD station site, the limestone section is probably only a few hundred meters thick, and the seismometer is probably very close to Precambrian basement. Very little crustal velocity information is available for the Black Hills region. Two seismic profiles in North Dakota and eastern Wyoming suggest the presence of a thick crust approximately 45 km thick in the vicinity of the Black Hills (Steinhart and Meyer, 1961).

Preliminary results at RSSD revealed extreme variations in the receiver functions with backazimuth (Figure 8; Owens *et al.*, 1983b). We attributed these variations to rapid changes in thickness and dip of sedimentary layers beneath RSSD. The effect on our analysis was to prevent detailed study of the deep crustal structure beneath the site. The dipping low-velocity wedge creates a strong azimuthal variation in

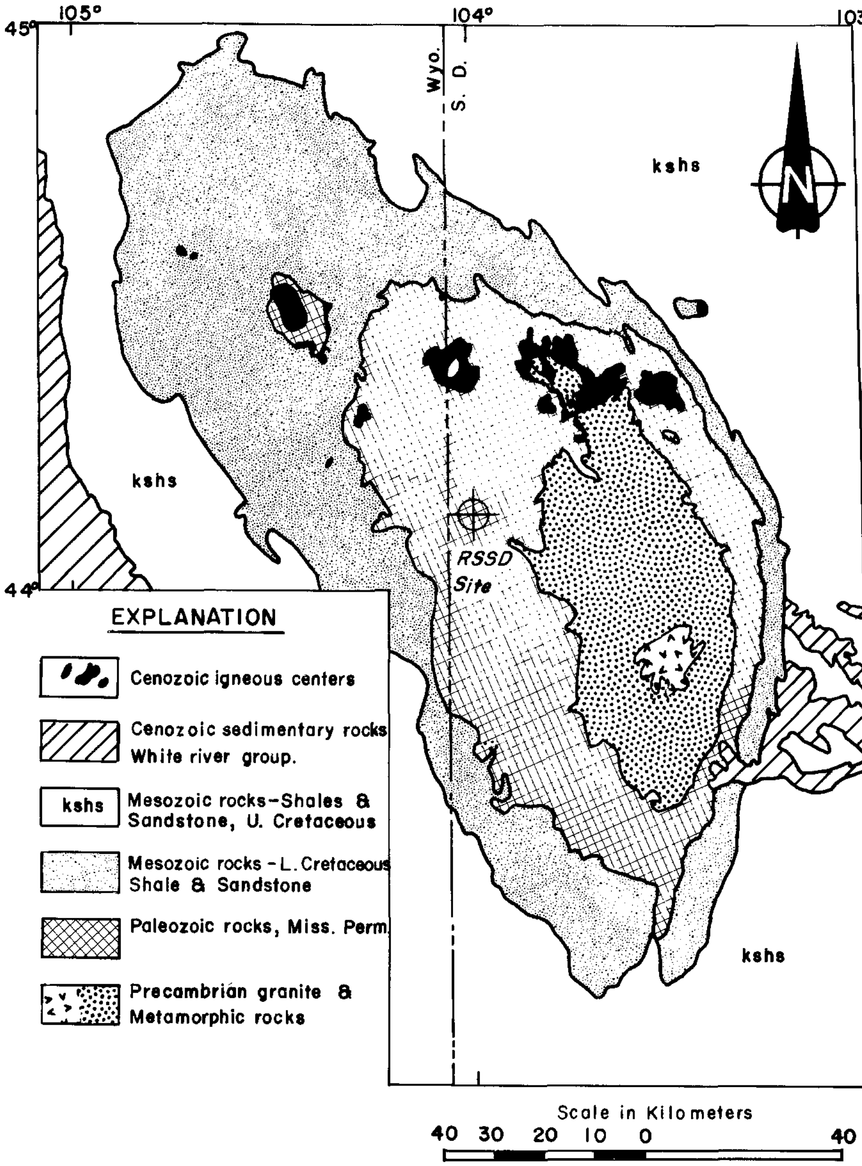

FIG. 7. Generalized geologic map of the RSSD site.

receiver functions at the station. The tangential component of motion is also large, with observed amplitudes approaching and, for some events, exceeding the amplitude of the radial component. The tangential receiver function from the north and southeast are nearly identical in the first few seconds except for a change in polarity (Figure 9), which is consistent with the generation of the tangential motion by a westward-dipping layer (Langston, 1977), as is the case at RSSD.

The complicated shallow structure as indicated by the large tangential components and markedly different radial receiver functions as a function of azimuth precludes an inversion for structure using a layered velocity model. However, we were able to obtain a first-order estimate of the crustal thickness at RSSD from possible *Ps* conversions identified from the southeast and southwest directions

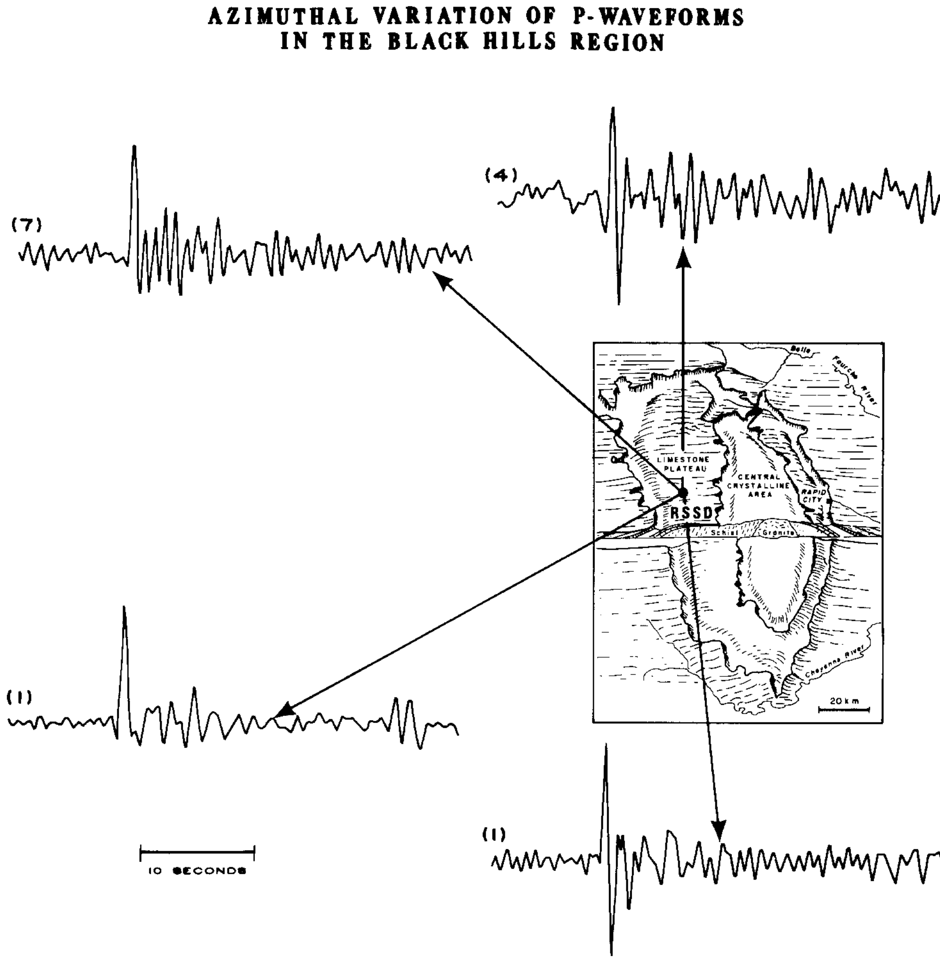

FIG. 8. Azimuthal variation in radial receiver functions around RSSD.

(Figure 8). The arrival time of the *Ps* phase is 5.9 ± 0.3 sec after the direct *P* wave. From this observation, we infer a crustal thickness of approximately 47 to 50 km beneath RSSD. The variation in *Ps* arrival time with azimuth probably indicates some structure on the Moho beneath the Black Hills, but the complex surface structure has prevented us from making a more detailed analysis at this time.

RSNY

The Precambrian (~1.1 Ga) Grenville Province, exposed in eastern Canada and the Adirondacks, extends southward in the subsurface to the west of the Appalachian mountain belt. The rocks of the Grenville Province are largely remobilized older basement of Superior or Hudsonian age and consist mainly of thick sequences of high-grade metasediments extensively intruded by granitic and anorthositic rocks. The Adirondack Mountains consist of a core of Precambrian Grenville rocks surrounded by gently dipping Paleozoic formations (Upper Cambria). In New York state, the Grenville crust appears to be uniform, about 36 km thick, with velocities ranging from 6.4 to 6.6 km/sec (Katz, 1955; Taylor *et al.*, 1980). The velocity models of Katz (1955) were determined from refraction lines extending from quarries in the central Adirondacks. The travel-time profiles were very straight, indicating a

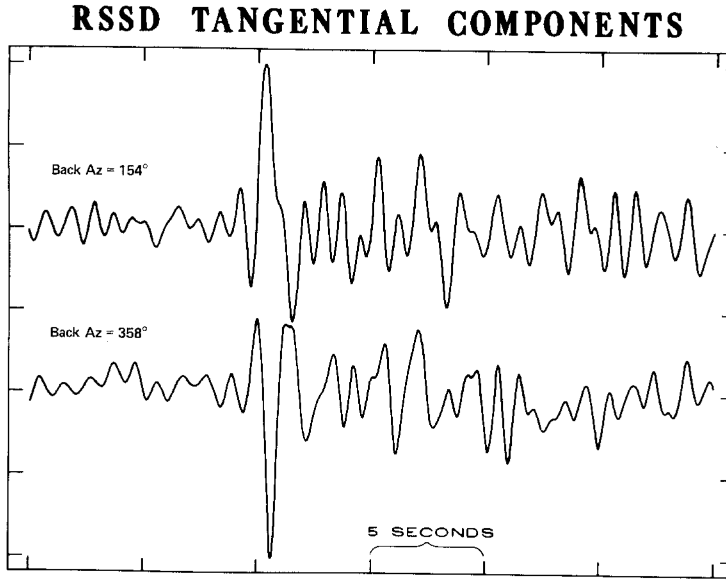

FIG. 9. Tangential receiver functions at two azimuths from RSSD showing similar, but opposite polarity, waveforms in the first 3 to 4 sec after the direct *P*.

uniform, unlayered crust, having average velocities of about 6.4 km/sec. The velocity of the Marcy anorthosite body was 6.6 km/sec, and the average crustal thickness was determined to be 35 km with upper mantle velocities of 8.1 km/sec. Taylor *et al.* (1980) also noted the apparent homogeneity of the Adirondack crust, especially in comparison with regional travel times in the New England Appalachians. They estimated the crust to be approximately 37 km thick with an average velocity of 6.6 km/sec, overlying an upper mantle with $Vp = 8.1$ km/sec.

Two investigations of crustal structure have been made in the Grenville Province in the northern Appalachians. Jordan and Frazer (1975) studied the *Sp* (*S* to *P*) conversions from two deep-focus South American earthquakes recorded at a number of long-period Canadian stations. Using forward modeling, the crustal thickness was estimated to be 35 km with surprisingly low shear velocities ($Vs = 3.4$ km/sec) in the lower crust. By comparing their estimated *Vs* with *P* velocities from nearby refraction models, a very high Poisson's ratio of 0.33 was calculated. Comparison with expected values of Poisson's ratio and *Vs* for rocks at 10 kbar suggested that hydrated ultramific rocks (serpentinized peridotite) may exist in the lower crust of the Grenville Province. Recent seismic reflection profiling by COCORP has shown that significant local variations in structure exist in the Adirondack region (Klemperer *et al.*, 1985). Of particular interest is the set of layered reflectors at depths of about 18 to 26 km depth, and the lack of Moho reflections.

We analyzed teleseismic *P* waveforms from four distinct backazimuths around RSNY (Figure 10). Data coverage was quite good for the northwest and south-southeast directions, while it was less extensive, but adequate, to the southwest and northeast. Detailed interpretation of the inversion results at RSNY is undertaken by Owens (1986) and is only summarized here. Inversion of the radial receiver functions produced good results at all backazimuths except the northeast, where the lack of clear arrivals made the inversion too dependent on the starting model. We can conclude from this that the crust and upper mantle northeast of RSNY

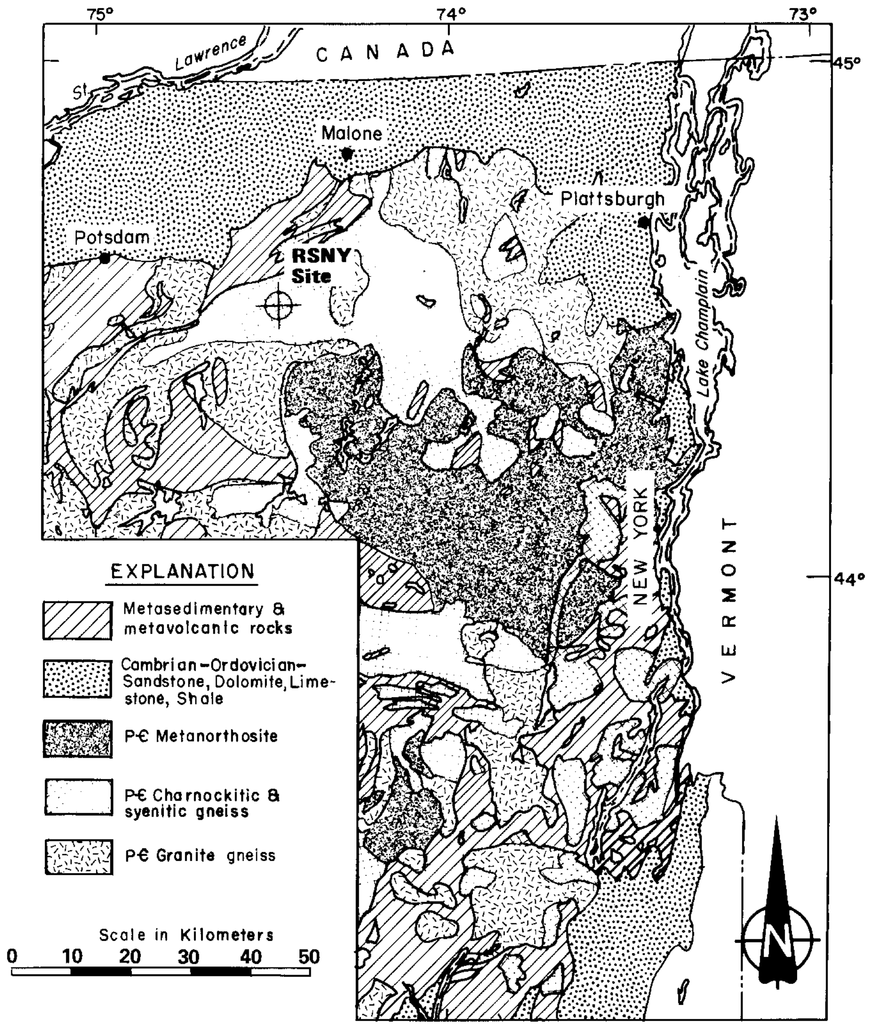

FIG. 10. Generalized geologic map of the RSNY site.

contains no velocity contrasts of sufficient magnitude to generate large converted phases.

The inversion of the south-southeast receiver function converged to a model whose response is an excellent fit to the observed data (Figure 11). The main features of the shear velocity model are first, upper crustal velocities (above 18 km depth) that are quite similar to those expected based on regional travel-time studies. Underlying this is a region of high shear velocities between 18 and 26 km depth that are anomalous relative to regional models. The well-constrained phases 2 to 4 and 10 to 15 sec after the direct *P* wave are generated by this prominent high-velocity zone. Below 26 km depth, the velocities are low (<3.7 km/sec) until 42 km, then they increase gradually. This is much different from previous studies, which indicate that a sharp crust-mantle boundary should exist at about 35 km depth. In actuality, the travel-time studies of Katz (1955) and Taylor *et al.* (1980) used simple 2- to 3-layer parameterizations to model observations, and no attempt was made to model a gradational crust-mantle boundary, although it could not be precluded from the data.

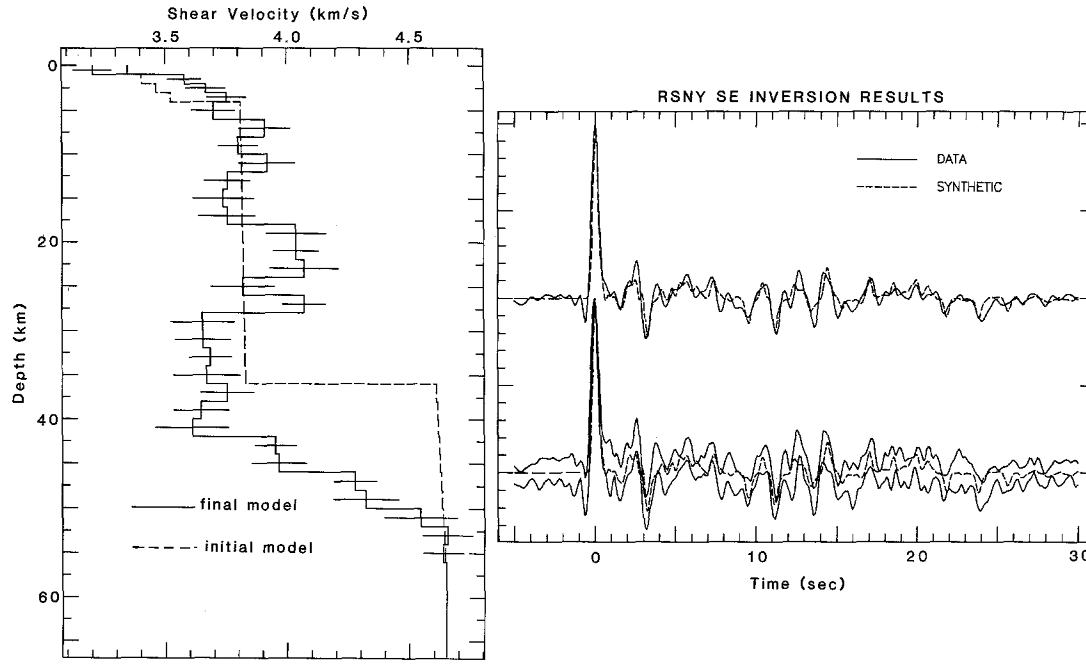

FIG. 11. RSNY south-southeast inversion results. *Left frame* shows the initial (dashed line) and final (solid line) shear velocity models. Approximate error bars of the final model are indicated for each layer. *Right frame* shows the fit of the final synthetic receiver function (dashed trace) to both the mean (upper solid trace) and bounding (lower two solid traces) receiver functions.

Inversions of southwest and northwest receiver functions also produced good fits to the observations, although the resulting models are somewhat different than our south-southeast results (Figure 12). Southwest of the site, there are slight complications due to shallow structure, but below 5 km the model is similar to the south-southeast in that a broad high-velocity zone exists (although it is not as prominent) and is underlain by a low-velocity zone and a thick crust-mantle transition zone. Northwest of the site, no high-velocity zone is present, and the structure of the crust-mantle boundary is different from the other azimuths, although the upper mantle velocities are still not apparent until about 50 km depth.

The results described above bear some interesting similarities with other data in the Adirondacks, but also raise important questions. Recall, our south-southeast results show a well-developed, high-velocity zone between 18 and 26 km depth. This zone is poorly developed southwest of RSNY, nearly absent northwest of the station and does not generate any converted phase energy in the northeast receiver function. As stated, this zone is not seen in results from regional travel-time studies. However, COCORP lines 7 and 11 (southeast of RSNY) indicates a highly reflective zone, termed the Tahawus complex by Klemperer *et al.* (1985), also at 18 to 26 km depth, while COCORP line 10 (west of RSNY) shows no evidence for this zone. The implications and interpretation of our high-velocity zone and Tahawus complex are obviously important to understanding the Adirondacks. In addition, there is an apparent correlation between these features, the low shear velocities in the lower crust and a large high electrical conductivity anomaly in the Adirondacks (Connerney *et al.*, 1980). These issues are discussed fully by Owens (1986). The point we wish to emphasize here is that the Tahawus complex appears to be characterized by high velocity and is a feature of limited lateral extent, although its boundaries

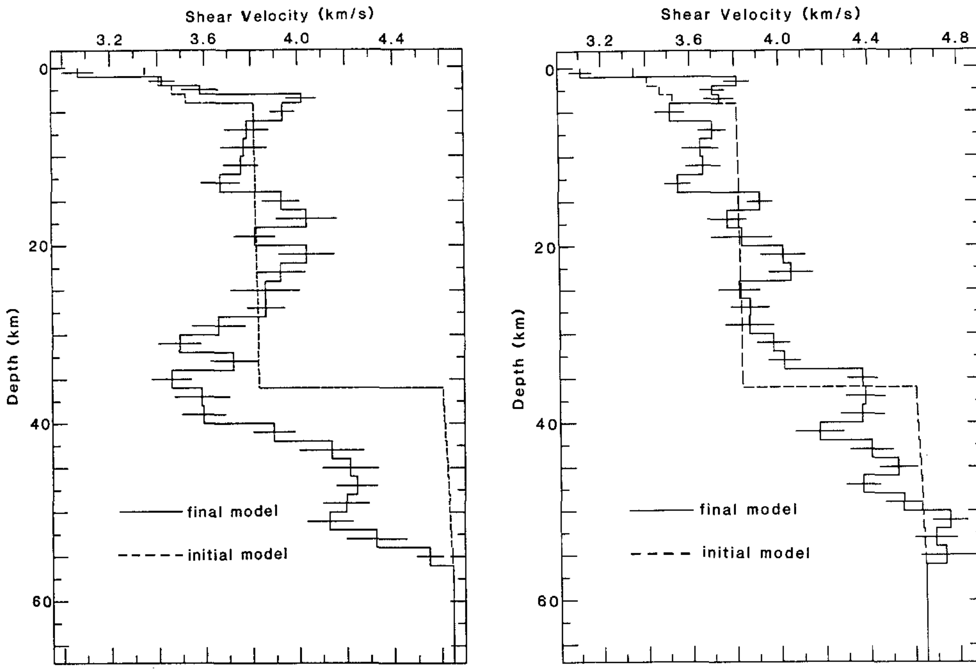

FIG. 12. Shear velocity models for the northwest (*right*) and southwest (*left*) backazimuths at RSNY. The solid line in each frame is the inversion result obtained using the initial model shown by the dashed line.

are not yet accurately defined. Such a feature would not appear in crustal models based on regional travel-time data. The regional crustal models of Katz (1955) and Taylor *et al.* (1980) available near RSNY adequately predict the overall average velocities of the crust found in our studies. However, broadband RSTN data is sensitive to variations in local structure on a scale that regional studies cannot resolve. Thus, site-specific methods such as teleseismic waveform modeling are important to accurately determine variations in structure very near the site. A major difference between the regional models and our models is the estimated crustal thickness. At all azimuths, our results suggest that upper mantle velocities with $Vs > 4.5$ km/sec do not occur until at least 50 km beneath RSNY. Regional models suggest the Moho should be at depths less than 40 km. Our results indicate that the transition from crustal to upper mantle velocities begins by 40 km depth, but is much more gradual.

RSON

Station RSON is located in the Precambrian Superior province of western Ontario (Figures 1 and 13; Taylor and Qualheim, 1983). Rocks in the station region typically give Archean ages between 2.7 and 3.1 b.y. The regional geology is characterized by a number of east-west trending bands of alternating greenstone belts (the Keewatin sequence) with intervening granitic masses. Station RSON is situated just north of the metasedimentary-gneiss terrain of the English River belt which lies between the Uchi volcanic belt to the north and the Wabigoon belt to the south. Geochemical analysis of the Keewatin volcanics indicate that they are of predominantly calc-alkaline affinity (Wilson *et al.*, 1965). This fact combined with additional structural and petrologic considerations suggest that Archean volcanic belts were once a series of island arcs separating thin crustal segments composed of sialic material.

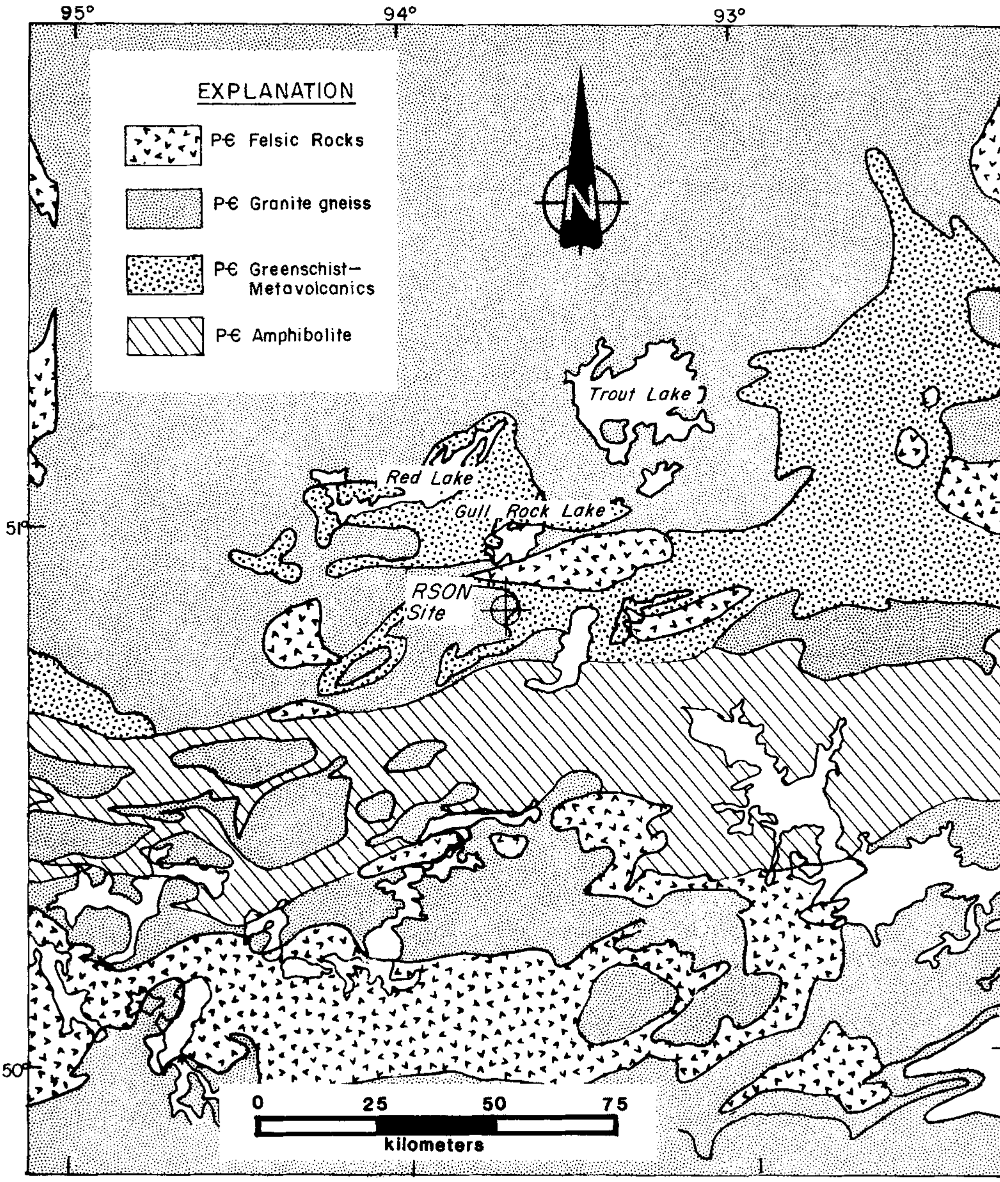

FIG. 13. Generalized geologic map of RSON.

A detailed deep seismic sounding experiment made in the vicinity of RSON suggests the presence of a two-layer crust with an average crustal thickness of approximately 35 km (Hall and Hajnal, 1969). A crustal section drawn through Red Lake shows an east-west trending upwarp in the Moho from a depth of about 39 km north of RSON to about 32 km to the south. A corresponding downwarp in the intermediate discontinuity was also found, which is centered over the English River gneissic belt described previously. To the northwest of Red Lake, a detailed study of the Superior-Churchill boundary zone indicates a 41-km-thick crust in the western Superior province that thickens to 46 km in the Churchill province (Green *et al.*, 1980). Also, the Churchill province appears to be characterized by a relatively high-velocity lower layer (~7 km/sec) that is absent in the Superior province. *Pn* velocities in the region appear to lie between 7.9 to 8.0 km/sec.

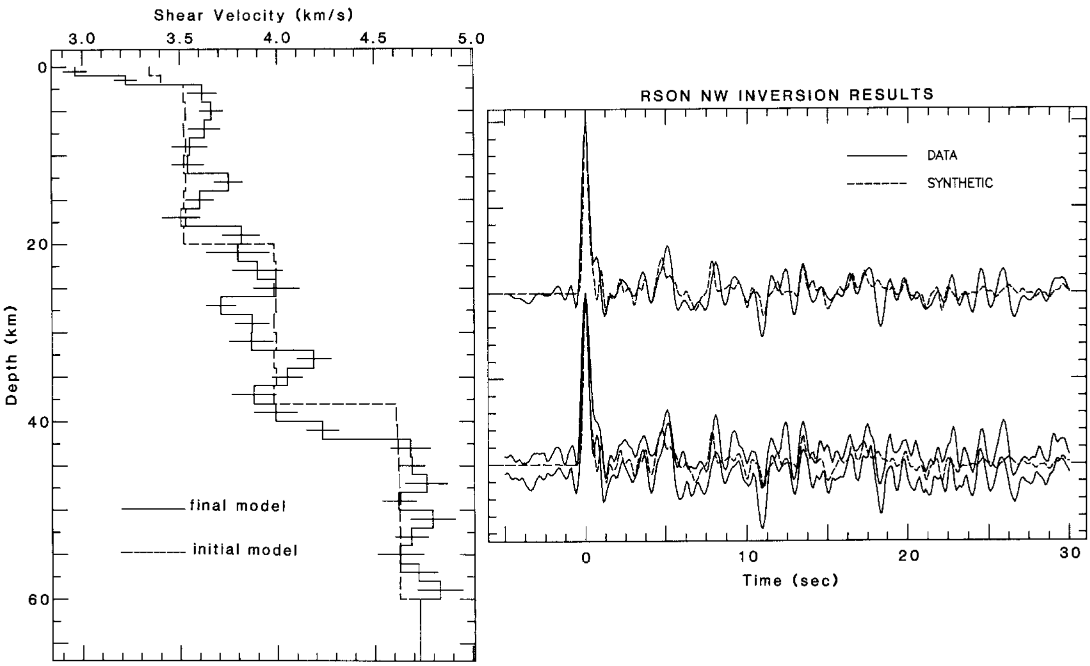

FIG. 14. RSON northwest inversion results. Same display scheme as Figure 11.

We obtained teleseismic receiver functions at RSON for 49 events. Most of these events were northwest (20 events) and south-southeast (16 events) of the site with several from the northeast and very few from the southwest. For this reason, we were not able to invert the southwest receiver functions, and we do not have good confidence in our northeast results. Our best results were obtained for the northwest direction (Figure 14). The starting model from Taylor and Qualheim (1983) is based on nearby refraction models which indicate a simple three-layer crust. Our results for the northwest azimuth confirm that the crust is fairly simple. We find a mid-crustal discontinuity at a slightly shallower depth (18 km) than the refraction model. It is not as large a velocity jump as the initial model, but it clearly separates upper crustal ($Vs < 3.7$ km/sec) from the lower crustal ($Vs > 3.9$ km/sec) velocities. On either side of this interface, the derived velocities vary but do not deviate significantly from the initial model. Our estimated crustal thickness is 42 km, slightly larger than the refraction model. The crust-mantle transition zone is only 2- to 4-km-thick, which is quite different from the RSNY and RSCP results.

The RSON northwest results are similar to our northeast and south-southeast results with only minor complications. Southeast results indicate that the increase from upper to lower crustal velocities occurs more gradually. In fact, between the surface and 36 km depth, the velocity increases nearly continuously. The crust-mantle transition is very similar to northwest results grading to upper mantle velocities over about 6 km depth with an estimated crustal thickness of 44 km. Although we do not have high confidence in our northeast inversion results due to the lack of high-quality events available for this analysis, inversion of the receiver functions produced results that do correlate with our other azimuths.

RSNT

Station RSNT is located at the southern edge of the Archean Slave Province in the northwestern part of the Canadian Shield (Figure 15; Taylor and Qualheim,

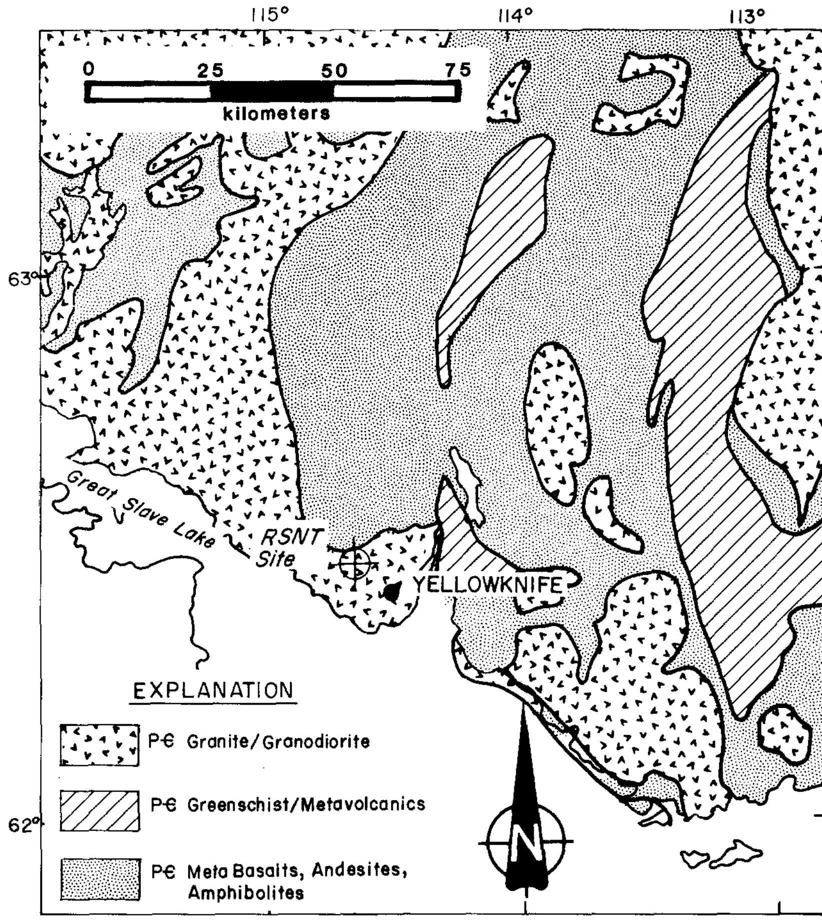

FIG. 15. Generalized geologic map of the RSNT site.

1983). Age dates in the region give values of approximately 2.5 b.y. The Slave Province consists of a number of northerly-trending, discontinuous greenstone belts (the Yellowknife Supergroup) separating large granitic regions. In contrast to the Superior Province, the volume of sedimentary rocks in the Slave Province greatly exceeds that of the volcanic rocks. Similar to other Archean terrains, the sedimentary sections are mainly composed of graywacke-mudstone turbidite sequences or their metamorphic equivalents. The volcanics are of a composition analogous to that of the Superior Province, and a similar tectonic evolution consisting of island arcs and thin, highly mobile continental fragments is implied.

Two major seismic refraction-reflection studies have been made in the vicinity of YKA (Barr, 1971; Clee *et al.*, 1974; Berry and Mair, 1977). These studies show some fairly strong lateral velocity variations in the upper crust just to the south of the array. A thin upper crustal low-velocity layer occurs in the granitic rocks beneath the array and is truncated just to the south beneath the Yellowknife Greenstone Belt. There is little evidence for a mid-crustal transition zone, and relatively low velocities of 6.2 to 6.4 km/sec are observed to the base of the crust. The Moho appears to be a complex transition zone, and the crustal thickness is about 32 km which is relatively thin for a shield region. However, the crust does appear to thicken to 36 km beneath the east arm of the Great Slave Lake which has been interpreted to be the site of a Proterozoic alacogen. The *Pn* velocity in the Slave Province is about 8.1 km/sec and increases to 8.23 km/sec just to the west of the Precambrian margin that lies west of YKA.

Because station RSNT is located far north and west of the other RSTN stations, it requires that somewhat different teleseismic source regions be used in our analysis. As a result, we have been able to develop receiver functions at three different distance ranges northwest of RSNT, but could not obtain sufficient events northeast and southwest of the site. In addition, we have enough events to invert south-southeast and due north of the site. The receiver functions for RSNT are all quite simple, the most simple of any RSTN site (see Figure 3). The only well-constrained phases present can be associated with the crust-mantle boundary. Initial forward modeling quickly determined that a crustal thickness of 32 km was too small to match the observed receiver functions without unrealistically low crustal velocities. Therefore, we modified the starting model for the inversions, so the Moho was at 36 km depth.

Inversion of the northwest receiver functions were done for three different stacking suites: distances from 48° to 55°; 61° to 71°; and 75° to 90°. The results for the closest distance range are shown in Figure 16. The constrained phases are matched well by the final model, which reflects the simplicity of the data in its nearly homogeneous crustal column. The crust-mantle transition is fairly sharp, spanning a depth range of 34 to 38 km. The average crustal shear velocities are low, but this is in agreement with low *P* velocities inferred from the refraction profiles.

The upper crustal models derived by inverting the other two distance ranges northwest of RSNT vary only slightly from the model presented here. However, the lowermost crust and crust-mantle transition undergo more significant changes. At the intermediate range, the velocity of the lower crust begins to increase as shallow as 30 km depth so that a much thicker crust-mantle transition is apparent. This

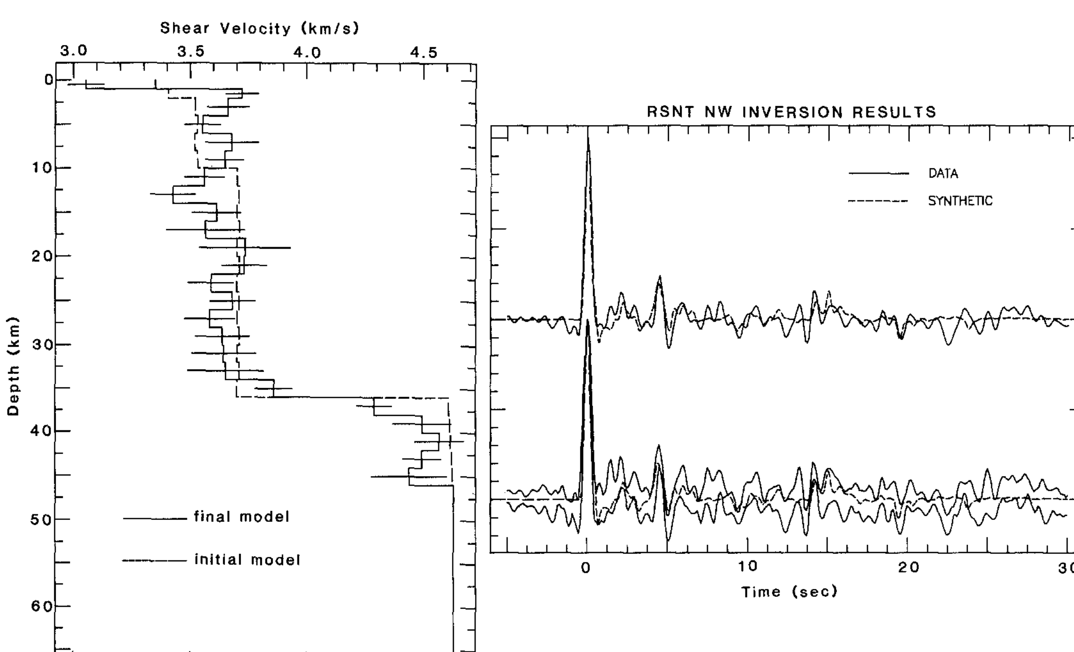

FIG. 16. RSNT northwest inversion results. Same display scheme as Figure 11.

transition extends to 38 km depth. Inversion of mean receiver function from distant events also yields a thick crust-mantle transition extending from 30 to 42 km depth. Despite these differences, all three distant ranges northwest of the site indicate that upper mantle velocities ($Vs > 4.5$ km/sec) do not occur until depths of 38 to 42 km, although the transition from the crust to the mantle could begin at depths as shallow as 30 km.

Discussion

A brief comparison of the results of our modeling of teleseismic *P* waveforms at RSTN sites provides an enlightening view of the capabilities and limitations of the technique. Application of the technique to the RSTN has allowed testing of its performance in a variety of conditions. Our most important observation is that, at sites where other seismic constraints exist, the structures inferred by teleseismic waveform modeling for the crust itself are in good agreement with the other studies. RSCP, although not discussed here, is the best example. Zandt and Owens (1986) found an excellent agreement between teleseismic waveform modeling results and those of refraction lines run directly over the site. At RSNY, we have inferred that our results appear to agree with two different types of seismic data. The average velocities seem to agree with regional travel-time studies, while aspects of the variation in detailed structure bears similarities to that inferred by COCORP deep reflection profiles (Owens, 1986).

However, the close correlation of teleseismic waveform modeling to other seismic results does not extend so nicely to the structure of the crust-mantle boundary. In every case except RSCP, the estimates of crustal thickness, defined here as the depth at which the shear velocities exceed 4.5 km/sec, are greater using teleseismic waveform modeling than using travel times of refracted seismic energy. An interesting aspect of this comparison is that the crustal thickness found by refraction techniques often correlates with the top of a crust-mantle transition zone in the receiver function inversion results.

Owens and Zandt (1985) examined the frequency-dependent behavior of converted phases from the crust-mantle boundary beneath three RSTN sites and found some interesting similarities between the transition zone models and realistic geologic models of the Moho. Among these similarities is that crust-mantle transition zones appear to be composed largely of material with velocities corresponding to mafic lower crustal rocks, while the actual change to velocities in the upper mantle range occurs rather abruptly (over about 3 km in depth) at the base of this zone. This implies that these transition zones should actually be included in estimates of the overall thickness in regions where they exist.

The apparent correlation of the top of crust-mantle transitions with estimates of crustal thickness from simple refraction travel-time analysis using only first arrival information suggests that there may be limitations to the resolution of these data in regions where such transition zones exist. On the other hand, the teleseismic waveform analysis results should also be scrutinized, since they require the assumption of horizontal homogeneous layers, which is clearly questionable within crust-mantle transition zones. The RSCP example illustrates that refraction and teleseismic methods can derive nearly identical results for the crust-mantle transition (Zandt and Owens, 1986). Since this is the only direct comparison in a region of overlapping data coverage currently available, some of the variations at other sites may be real differences in the structure between the location where each data set was obtained. However, the apparent overestimation of crustal thickness by teleseismic waveform analysis relative to the thickness found by refraction analysis should be more completely studied because of the importance placed on seismically determined crustal thickness in tectonic problems.

CONCLUSIONS

The crust and upper-mantle velocity structure beneath five broadband seismic stations of the RSTN have been estimated from inversion of stacked teleseismic receiver functions. In regions characterized by relatively simple geologic structure, detailed velocity models can be obtained that generally show good correspondence with nearby high resolution refraction and reflection data. Lateral variations in structure around a site can be studied by inverting waveforms from various azimuths and from observations of tangential receiver functions.

With the exception of RSSD (in the Black Hills, South Dakota), the RSTN sites are characterized by relatively simple structure. This result is not unexpected due to their location in Precambrian shield regions. Station RSCP (Cumberland Plateau, Tennessee) exhibits the most complex waveforms which are due to the presence of late Paleozoic sedimentary sequences and the southern termination of a Precambrian rift system just to the northeast. A gradational crust-mantle boundary is observed beneath RSCP, and the derived velocity structure shows an impressive correlation with a detailed interpretation of reversed refraction lines. A gradational Moho is also observed beneath the RSNY station in the Adirondacks, and a high-velocity region in the mid-crust correlates well with a set of high-amplitude reflectors obtained from nearby COCORP lines. The crust beneath RSON and RSNT are relatively simple as evidenced by the uncomplicated receiver functions. In both regions, the crust-mantle boundary is abrupt, and RSNT is characterized by a remarkably simple crustal structure. The crustal thicknesses at each of these sites are: RSCP, 40 to 50 km; RSSD, 47 to 50 km; RSNY, 45 to 50 km; RSNT, 38 km; and RSON, 42 km.

ACKNOWLEDGMENTS

The University of Missouri Geology Department Fund supported preparation of the figures for this paper. This research was supported by Lawrence Livermore National Laboratory through the Department of Energy Contract W-7405-ENG-48.

REFERENCES

Barr, K. G. (1971). Crustal refraction experiment: Yellowknife, 1966, *J. Geophys. Res.* **76,** 1929–1947.

Berry, M. J. and J. A. Mair (1977). The nature of the Earth's crust, in *Canada AGU Geophys. Mon. 20,* J. G. Heacock, Editor, Washington, D.C., 319–348.

Borcherdt, R. D. and Roller, J. C. (1966). A preliminary summary of a seismic-refraction survey in the vicinity of the Cumberland Plateau Observatory, Tennessee, *U.S. Geol. Surv., Tech. Letter 43,* 31 pp.

Clee, T. E., K. G. Barr, and M. J. Berry (1974). Fine structure of the crust near Yellowknife, *Can J. Earth Sci.* **11,** 1534–1544.

Connerney, J. E. P., A. Nekut, and A. F. Kuckes (1980). Deep crustal electrical conductivity in the Adirondacks, *J. Geophys. Res.* **85,** 2602–2614.

Cook, F. A., D. S. Albough, L. D. Brown, S. Kaufman, J. E. Oliver, and R. D. Hatcher (1979). Thin-skinned tectonics in the crystalline southern Appalachians: COCORP seismic-reflection profiling of the Blue Ridge and Piedmont, *Geology* **7,** 563–567.

Green, A. G., O. G. Stephenson, G. D. Mann, E. R. Kanasewich, G. L. Cumming, Z. Hajnal, J. A. Mair, and G. F. West (1980). Cooperative seismic surveys across the Superior-Churchill boundary zone in southern Canada, *Can J. Earth Sci.* **17,** 617–632.

Hall, D. H. and J. Hajnal (1969). Crustal structure of northwestern Ontario: refraction seismology, *Can J. Earth Sci.* **6,** 81–99.

Hatcher, R. D. (1978). Tectonics of the western Piedmont and Blue Ridge, southern Appalachians: review and speculation, *Am. J. Sci.* **78,** 276–304.

Jordan, T. H. and L. N. Frazer (1975). Crustal and upper-mantle structure from *Sp* phases, *J. Geophys. Res.* **80,** 1504–1518.

Katz, S. (1955). Seismic study of crustal structure in Pennsylvania and New York, *Bull. Seism. Soc. Am.* **45,** 303–325.

Keller, G. R., A. E. Bland, and J. K. Greenberg (1982). Evidence for a major late Precambrian tectonic event (rifting) in the eastern midcontinent region, United States, *Tectonics* **1,** 213–223.

Klemperer, S. L., L. D. Brown, J. E. Oliver, C. J. Ando, B. L. Czuchra, and S. Kaufman (1985). Some results of COCORP seismic reflection profiling in the Grenville-age Adirondack mountains, New York State, *Can J. Earth Sci.* **22,** 141–153.

Langston, C. A. (1977). The effect of planar dipping structure on source and receiver responses for constant ray parameter, *Bull. Seism. Soc. Am.* **67,** 1029–1050.

Langston, C. A. (1979). Structure under Mount Rainier, Washington, inferred from teleseismic body waves, *J. Geophys. Res.* **84,** 4749–4762.

Owens, T. J. (1984). Determination of crustal and upper mantle structure from analysis of broadband teleseismic *P*-waveforms, *Ph.D. Dissertation*, University of Utah, Provo, Utah, 146 pp.

Owens, T. J. (1986). Crustal structure of the Adirondack mountains determined from broadband teleseismic waveform modeling (submitted for publication).

Owens, T. J. and G. Zandt (1985). The response of the continental crust-mantle boundary observed on broadband teleseismic receiver functions, *Geophys. Res. Letters* **12,** 705–708.

Owens, T. J., S. R. Taylor, and G. Zandt (1983a). Isolation and enhancement of the response of local seismic structure from teleseismic *P*-waveforms, Rept. UCID-19809, Lawrence Livermore National Laboratory, Livermore, California, 33 pp.

Owens, T. J., S. R. Taylor, and G. Zandt (1983b). Crustal structure beneath RSNT stations inferred from teleseismic *P*-waveforms: preliminary results at RSCP, RSSD, and RSNY, Rept. UCID-19859, Lawrence Livermore National Laboratory, Livermore, California, 28 pp.

Owens, T. J., G. Zandt, and S. R. Taylor (1984). Seismic evidence for an ancient rift beneath the Cumberland Plateau, TN: a detailed analysis of broadband teleseismic *P*-waveforms, *J. Geophys. Res.* **89,** 7783–7795.

Prodehl, C., J. Schlittenhardt, and S. W. Stewart (1984). Crustal structure of the Appalachian highlands in Tennessee, *Tectonophysics* **109,** 61–76.

Steinhart, J. S. and R. P. Meyer (1961). Explosion studies of continental structure: Washington, D.C., *Carnegie Institute of Washington Publication 622*, 409.

Taylor, S. R. and B. J. Qualheim (1983). RSTN site descriptions, Rept. UCID-19769, Lawrence Livermore National Laboratory, Livermore, California, 79 pp.

Taylor, S. R. and T. J. Owens (1984). Inversion of receiver transfer functions for crustal structure, *Earthquake Notes* **55,** 5–12.

Taylor, S. R., M. N. Töksoz, and M. P. Chaplin (1980). Crustal structure of the northeastern United States: contrasts between Grenville and Appalachian provinces, *Science* **208,** 595–597.

Zandt, G. and T. J. Owens (1986). Comparison of crustal velocity profiles determined by seismic refraction and teleseismic methods, *Tectonophysics* **128,** 151–161.

Earth Science Division
Lawrence Livermore National Laboratory
Livermore, California 94550

Manuscript received 28 July 1986

Appendix: Tables of Velocity Models for RSTN Sites

The following 11 tables are the inversion results for all RSTN stations except RSSD. The backazimuth for each table indicates the direction from the station to the events which formed the stacking suite for that case.

TABLE A1

RSCP SOUTH-SOUTHEAST BACKAZIMUTH

Layer	*P* Velocity (km/sec)	*S* Velocity (km/sec)	Density (gm/cm^3)	Depth to Top (km)	Layer Thickness (km)
1	3.77	2.18	2.50	0.0	1.7
2	6.29	3.64	2.78	1.7	2.5
3	6.12	3.54	2.72	4.2	2.5
4	6.36	3.68	2.80	6.7	2.5
5	6.45	3.73	2.83	9.2	2.5
6	6.40	3.70	2.81	11.7	3.0
7	6.47	3.74	2.84	14.7	2.5
8	6.87	3.97	2.96	17.2	2.5
9	6.85	3.96	2.96	19.7	2.5
10	6.85	3.96	2.96	22.2	2.5
11	6.65	3.85	2.90	24.7	2.5
12	6.85	3.96	2.96	27.2	2.5
13	7.01	4.06	3.01	29.7	2.5
14	6.59	3.81	2.88	32.2	2.5
15	6.56	3.80	2.87	34.7	2.5
16	6.82	3.95	2.95	37.2	2.5
17	7.18	4.15	3.07	39.7	1.5
18	7.33	4.24	3.11	42.2	1.5
19	7.28	4.21	3.10	43.7	1.5
20	7.26	4.20	3.09	45.2	1.5
21	7.73	4.47	3.24	46.7	1.5
22	7.81	4.52	3.27	48.2	1.5
23	7.61	4.40	3.20	49.7	1.5
24	8.00	4.62	3.33	51.2	1.5
25	8.01	4.63	3.33	52.7	2.5
26	8.55	4.94	3.50	55.2	2.5
27	8.36	4.84	3.44	57.7	2.5
28	8.15	4.71	3.38	60.2	∞

TABLE A2

RSCP Northeast Backazimuth

Layer	P Velocity (km/sec)	S Velocity (km/sec)	Density (gm/cm^3)	Depth to Top (km)	Layer Thickness (km)
1	3.69	2.14	2.70	0.0	1.7
2	5.92	3.42	2.66	1.7	2.5
3	5.86	3.39	2.65	4.2	2.5
4	5.85	3.38	2.64	6.7	2.5
5	6.10	3.53	2.72	9.2	2.5
6	6.11	3.53	2.72	11.7	3.0
7	6.92	4.00	2.98	14.7	2.5
8	7.06	4.08	3.03	17.2	2.5
9	7.18	4.15	3.06	19.7	2.5
10	6.64	3.84	2.89	22.2	2.5
11	6.48	3.75	2.84	24.7	2.5
12	6.86	3.97	2.96	27.2	2.5
13	6.81	3.94	2.95	29.7	2.5
14	6.90	3.99	2.98	32.2	2.5
15	6.88	3.98	2.97	34.7	2.5
16	7.20	4.16	3.07	37.2	2.5
17	7.43	4.30	3.14	39.7	1.5
18	7.34	4.24	3.12	42.2	1.5
19	7.68	4.44	3.23	43.7	1.5
20	7.30	4.22	3.10	45.2	1.5
21	7.36	4.25	3.12	46.7	1.5
22	7.13	4.12	3.05	48.2	1.5
23	7.66	4.43	3.22	49.7	1.5
24	7.74	4.48	3.24	51.2	1.5
25	8.01	4.63	3.33	52.7	2.5
26	7.91	4.57	3.30	55.2	2.5
27	8.21	4.75	3.39	57.7	2.5
28	8.15	4.71	3.38	60.2	∞

TABLE A3

RSNY SOUTH-SOUTHEAST BACKAZIMUTH

Layer	*P* Velocity (km/sec)	*S* Velocity (km/sec)	Density (gm/cm^3)	Depth to Top (km)	Layer Thickness (km)
1	5.54	3.20	2.54	0.0	1.0
2	6.19	3.58	2.75	1.0	1.0
3	6.34	3.66	2.79	2.0	1.0
4	6.49	3.75	2.84	3.0	1.0
5	6.40	3.70	2.81	4.0	2.0
6	6.76	3.91	2.93	6.0	2.0
7	6.57	3.80	2.87	8.0	2.0
8	6.77	3.92	2.93	10.0	2.0
9	6.49	3.75	2.84	12.0	2.0
10	6.46	3.73	2.84	14.0	2.0
11	6.49	3.75	2.84	16.0	2.0
12	6.99	4.04	3.01	18.0	2.0
13	6.99	4.04	3.01	20.0	2.0
14	7.02	4.06	3.02	22.0	2.0
15	6.60	3.81	2.88	24.0	2.0
16	7.02	4.06	3.02	26.0	2.0
17	6.31	3.65	2.79	28.0	2.0
18	6.31	3.65	2.79	30.0	2.0
19	6.37	3.68	2.81	32.0	2.0
20	6.34	3.66	2.80	34.0	2.0
21	6.49	3.75	2.84	36.0	2.0
22	6.30	3.64	2.78	38.0	2.0
23	6.24	3.61	2.76	40.0	2.0
24	6.83	3.95	2.95	42.0	2.0
25	6.86	3.96	2.96	44.0	2.0
26	7.40	4.27	3.13	46.0	2.0
27	7.47	4.32	3.16	48.0	2.0
28	7.86	4.54	3.28	50.0	2.0
29	8.05	4.65	3.34	52.0	2.0
30	8.02	4.63	3.33	54.0	2.0
31	8.20	4.65	3.35	56.0	∞

TABLE A4

RSNY Northwest Backazimuth

Layer	P Velocity (km/sec)	S Velocity (km/sec)	Density (gm/cm^3)	Depth to Top (km)	Layer Thickness (km)
1	5.38	3.11	2.49	0.0	1.0
2	6.59	3.81	2.88	1.0	1.0
3	6.40	3.70	2.81	2.0	1.0
4	6.45	3.73	2.83	3.0	1.0
5	6.07	3.51	2.71	4.0	2.0
6	6.40	3.70	2.82	6.0	2.0
7	6.31	3.65	2.79	8.0	2.0
8	6.32	3.66	2.80	10.0	2.0
9	6.12	3.54	2.73	12.0	2.0
10	6.76	3.91	2.93	14.0	2.0
11	6.50	3.76	2.85	16.0	2.0
12	6.61	3.82	2.88	18.0	2.0
13	6.94	4.01	2.99	20.0	2.0
14	7.00	4.04	3.01	22.0	2.0
15	6.60	3.81	2.88	24.0	2.0
16	6.68	3.86	2.90	26.0	2.0
17	6.67	3.85	2.90	28.0	2.0
18	6.86	3.96	2.96	30.0	2.0
19	6.95	4.01	2.99	32.0	2.0
20	7.56	4.37	3.19	34.0	2.0
21	7.58	4.38	3.20	36.0	2.0
22	7.56	4.37	3.19	38.0	2.0
23	7.22	4.17	3.08	40.0	2.0
24	7.62	4.40	3.21	42.0	2.0
25	7.82	4.52	3.27	44.0	2.0
26	7.55	4.36	3.18	46.0	2.0
27	7.87	4.55	3.28	48.0	2.0
28	8.23	4.75	3.40	50.0	2.0
29	8.12	4.69	3.36	52.0	2.0
30	8.19	4.73	3.39	54.0	2.0
31	8.20	4.65	3.35	56.0	∞

TABLE A5

RSNY Southwest Backazimuth

Layer	P Velocity (km/sec)	S Velocity (km/sec)	Density (gm/cm^3)	Depth to Top (km)	Layer Thickness (km)
1	5.30	3.06	2.46	0.0	1.0
2	5.91	3.42	2.66	1.0	1.0
3	6.19	3.58	2.75	2.0	1.0
4	6.94	4.01	2.99	3.0	1.0
5	6.80	3.93	2.94	4.0	2.0
6	6.54	3.78	2.86	6.0	2.0
7	6.51	3.76	2.85	8.0	2.0
8	6.49	3.75	2.84	10.0	2.0
9	6.34	3.66	2.80	12.0	2.0
10	6.79	3.92	2.94	14.0	2.0
11	6.98	4.03	3.00	16.0	2.0
12	6.59	3.81	2.88	18.0	2.0
13	6.98	4.03	3.00	20.0	2.0
14	6.78	3.92	2.94	22.0	2.0
15	6.67	3.85	2.90	24.0	2.0
16	6.67	3.85	2.90	26.0	2.0
17	6.32	3.65	2.79	28.0	2.0
18	6.03	3.48	2.70	30.0	2.0
19	6.44	3.72	2.83	32.0	2.0
20	5.98	3.45	2.68	34.0	2.0
21	6.20	3.58	2.75	36.0	2.0
22	6.21	3.59	2.75	38.0	2.0
23	6.73	3.89	2.92	40.0	2.0
24	7.15	4.13	3.06	42.0	2.0
25	7.29	4.21	3.10	44.0	2.0
26	7.33	4.24	3.11	46.0	2.0
27	7.26	4.19	3.09	48.0	2.0
28	7.14	4.12	3.05	50.0	2.0
29	7.48	4.32	3.16	52.0	2.0
30	7.87	4.55	3.28	54.0	2.0
31	8.20	4.65	3.35	56.0	∞

TABLE A6

RSON South-Southeast Backazimuth

Layer	P Velocity (km/sec)	S Velocity (km/sec)	Density (gm/cm^3)	Depth to Top (km)	Layer Thickness (km)
1	5.74	3.32	2.60	0.0	1.0
2	5.64	3.26	2.57	1.0	1.0
3	6.24	3.60	2.76	2.0	2.0
4	6.30	3.64	2.78	4.0	2.0
5	6.09	3.52	2.72	6.0	2.0
6	5.94	3.43	2.67	8.0	2.0
7	6.17	3.57	2.74	10.0	2.0
8	6.18	3.57	2.74	12.0	2.0
9	6.41	3.70	2.82	14.0	2.0
10	6.30	3.64	2.78	16.0	2.0
11	6.36	3.67	2.80	18.0	2.0
12	6.37	3.68	2.81	20.0	2.0
13	6.31	3.64	2.79	22.0	2.0
14	6.53	3.77	2.86	24.0	2.0
15	6.71	3.87	2.91	26.0	2.0
16	6.86	3.96	2.96	28.0	2.0
17	6.71	3.87	2.91	30.0	2.0
18	6.59	3.81	2.87	32.0	2.0
19	6.87	3.97	2.97	34.0	2.0
20	7.11	4.11	3.04	36.0	2.0
21	7.08	4.09	3.03	38.0	2.0
22	7.53	4.35	3.18	40.0	2.0
23	7.59	4.38	3.20	42.0	2.0
24	8.09	4.68	3.36	44.0	2.0
25	8.06	4.66	3.35	46.0	2.0
26	7.66	4.43	3.22	48.0	2.0
27	8.03	4.64	3.34	50.0	2.0
28	8.15	4.71	3.37	52.0	2.0
29	8.39	4.85	3.45	54.0	2.0
30	8.30	4.80	3.42	56.0	2.0
31	8.28	4.78	3.42	58.0	2.0
32	8.20	4.73	3.35	60.0	∞

TABLE A7

RSON NORTHWEST BACKAZIMUTH

Layer	*P* Velocity (km/sec)	*S* Velocity (km/sec)	Density (gm/cm^3)	Depth to Top (km)	Layer Thickness (km)
1	5.12	2.96	2.41	0.0	1.0
2	5.57	3.22	2.55	1.0	1.0
3	6.25	3.61	2.77	2.0	2.0
4	6.33	3.66	2.79	4.0	2.0
5	6.27	3.62	2.77	6.0	2.0
6	6.14	3.55	2.73	8.0	2.0
7	6.12	3.54	2.73	10.0	2.0
8	6.48	3.75	2.84	12.0	2.0
9	6.23	3.60	2.76	14.0	2.0
10	6.06	3.50	2.71	16.0	2.0
11	6.60	3.81	2.88	18.0	2.0
12	6.57	3.79	2.87	20.0	2.0
13	6.74	3.89	2.92	22.0	2.0
14	6.91	3.99	2.98	24.0	2.0
15	6.42	3.71	2.82	26.0	2.0
16	6.69	3.87	2.91	28.0	2.0
17	6.68	3.86	2.91	30.0	2.0
18	7.24	4.18	3.08	32.0	2.0
19	7.00	4.05	3.01	34.0	2.0
20	6.71	3.87	2.91	36.0	2.0
21	6.90	3.99	2.98	38.0	2.0
22	7.32	4.23	3.11	40.0	2.0
23	8.10	4.68	3.36	42.0	2.0
24	8.11	4.69	3.36	44.0	2.0
25	8.24	4.76	3.40	46.0	2.0
26	7.99	4.62	3.33	48.0	2.0
27	8.29	4.79	3.42	50.0	2.0
28	8.10	4.68	3.36	52.0	2.0
29	8.01	4.63	3.33	54.0	2.0
30	8.16	4.72	3.38	56.0	2.0
31	8.36	4.83	3.44	58.0	2.0
32	8.20	4.73	3.35	60.0	∞

TABLE A8

RSNT South-Southeast Backazimuth

Layer	P Velocity (km/sec)	S Velocity (km/sec)	Density (gm/cm^3)	Depth to Top (km)	Layer Thickness (km)
1	5.44	3.14	2.51	0.0	1.0
2	6.17	3.56	2.74	1.0	1.0
3	6.36	3.67	2.80	2.0	2.0
4	5.97	3.45	2.68	4.0	2.0
5	5.71	3.30	2.60	6.0	2.0
6	5.66	3.27	2.58	8.0	2.0
7	5.91	3.41	2.66	10.0	2.0
8	5.87	3.39	2.65	12.0	2.0
9	6.10	3.52	2.72	14.0	2.0
10	6.24	3.61	2.77	16.0	2.0
11	6.34	3.66	2.79	18.0	2.0
12	6.37	3.68	2.81	20.0	2.0
13	6.25	3.61	2.77	22.0	2.0
14	6.57	3.79	2.87	24.0	2.0
15	6.50	3.76	2.85	26.0	2.0
16	6.64	3.84	2.89	28.0	2.0
17	6.80	3.93	2.94	30.0	2.0
18	6.90	3.98	2.97	32.0	2.0
19	7.02	4.05	3.01	34.0	2.0
20	6.84	3.95	2.96	36.0	2.0
21	7.11	4.11	3.04	38.0	2.0
22	7.10	4.10	3.04	40.0	2.0
23	7.15	4.13	3.06	42.0	2.0
24	7.82	4.52	3.27	44.0	2.0
25	8.10	4.63	3.34	46.0	∞

TABLE A9

RSNT Northeast Backazimuth

Layer	*P* Velocity (km/sec)	*S* Velocity (km/sec)	Density (gm/cm^3)	Depth to Top (km)	Layer Thickness (km)
1	4.99	2.88	2.36	0.0	1.0
2	5.86	3.39	2.64	1.0	1.0
3	6.17	3.57	2.74	2.0	2.0
4	5.85	3.38	2.64	4.0	2.0
5	5.92	3.42	2.66	6.0	2.0
6	5.81	3.36	2.63	8.0	2.0
7	6.29	3.63	2.78	10.0	2.0
8	6.08	3.51	2.71	12.0	2.0
9	6.42	3.71	2.82	14.0	2.0
10	6.44	3.72	2.83	16.0	2.0
11	6.19	3.57	2.75	18.0	2.0
12	6.46	3.73	2.83	20.0	2.0
13	6.32	3.65	2.79	22.0	2.0
14	6.37	3.68	2.81	24.0	2.0
15	6.37	3.68	2.81	26.0	2.0
16	6.41	3.70	2.82	28.0	2.0
17	6.83	3.95	2.95	30.0	2.0
18	7.00	4.05	3.01	32.0	2.0
19	6.99	4.04	3.00	34.0	2.0
20	7.36	4.25	3.12	36.0	2.0
21	7.55	4.36	3.18	38.0	2.0
22	7.67	4.43	3.22	40.0	2.0
23	7.70	4.45	3.23	42.0	2.0
24	8.00	4.62	3.33	44.0	2.0
25	8.10	4.63	3.34	46.0	∞

TABLE A10

RSNT Northwest Backazimuth—Distance Range 75° to 90°

Layer	P Velocity (km/sec)	S Velocity (km/sec)	Density (gm/cm^3)	Depth to Top (km)	Layer Thickness (km)
1	5.33	3.08	2.47	0.0	1.0
2	5.99	3.46	2.68	1.0	1.0
3	6.46	3.73	2.83	2.0	2.0
4	6.38	3.69	2.81	4.0	2.0
5	6.41	3.70	2.82	6.0	2.0
6	6.03	3.48	2.70	8.0	2.0
7	5.88	3.40	2.65	10.0	2.0
8	6.08	3.51	2.71	12.0	2.0
9	5.94	3.43	2.67	14.0	2.0
10	6.23	3.60	2.76	16.0	2.0
11	6.28	3.63	2.78	18.0	2.0
12	6.37	3.68	2.81	20.0	2.0
13	6.26	3.61	2.77	22.0	2.0
14	6.33	3.66	2.79	24.0	2.0
15	6.20	3.58	2.75	26.0	2.0
16	6.42	3.71	2.82	28.0	2.0
17	6.94	4.01	2.99	30.0	2.0
18	7.01	4.05	3.01	32.0	2.0
19	7.24	4.18	3.08	34.0	2.0
20	7.54	4.36	3.18	36.0	2.0
21	7.71	4.46	3.24	38.0	2.0
22	7.90	4.57	3.30	40.0	2.0
23	8.09	4.68	3.36	42.0	2.0
24	7.86	4.54	3.28	44.0	2.0
25	8.10	4.63	3.34	46.0	∞

TABLE A11

RSNT NORTHWEST BACKAZIMUTH—DISTANCE RANGE 61° TO 71°

Layer	*P* Velocity (km/sec)	*S* Velocity (km/sec)	Density (gm/cm^3)	Depth to Top (km)	Layer Thickness (km)
1	5.16	2.98	2.42	0.0	1.0
2	6.12	3.53	2.72	1.0	1.0
3	6.41	3.71	2.82	2.0	2.0
4	6.34	3.66	2.79	4.0	2.0
5	6.56	3.79	2.87	6.0	2.0
6	6.22	3.59	2.76	8.0	2.0
7	5.94	3.43	2.67	10.0	2.0
8	5.84	3.37	2.64	12.0	2.0
9	5.83	3.37	2.63	14.0	2.0
10	6.20	3.58	2.75	16.0	2.0
11	6.32	3.65	2.79	18.0	2.0
12	6.29	3.63	2.78	20.0	2.0
13	6.02	3.48	2.69	22.0	2.0
14	6.20	3.58	2.75	24.0	2.0
15	6.13	3.54	2.73	26.0	2.0
16	6.13	3.54	2.73	28.0	2.0
17	6.57	3.79	2.87	30.0	2.0
18	6.68	3.86	2.90	32.0	2.0
19	7.07	4.08	3.03	34.0	2.0
20	7.78	4.49	3.26	36.0	2.0
21	8.00	4.62	3.33	38.0	2.0
22	8.04	4.65	3.34	40.0	2.0
23	7.77	4.49	3.25	42.0	2.0
24	7.87	4.55	3.28	44.0	2.0
25	8.10	4.63	3.34	46.0	∞